ACS Electrochemistry



pubs.acs.org/electrochem
Article

# Quaternary Ammonium Additives as Dual Inhibitors of Hydrogen Evolution and Cathodic Corrosion in Aqueous Electrosynthesis

Achanta K. S. Koushik, Pietro Vannini, Eva Plut, Wiebke Jansen, Siegfried R. Waldvogel,* and Jean-Philippe Tessonnier*

Cite This: ACS Electrochem. 2026, 2, 175−187
Read Online



**ABSTRACT:** In organic electrosynthesis, the hydrogen evolution reaction (HER) is a parasitic process that significantly diminishes the faradaic efficiency (FE) of aqueous electrochemical reductions and contributes to the cathodic corrosion of widely used metals such as lead and tin. Developing strategies that selectively suppress HER without hindering desired electrochemical transformations is therefore crucial. In this study, we demonstrate that various quaternary ammonium salts (QAS) suppress HER on lead cathodes even under acidic conditions (pH 1). These QAS electrostatically self-assemble at the negatively charged lead surface, forming a cationic barrier that hinders hydronium ion ($H_3O^+$) diffusion to the surface, thereby mitigating HER. Chronoamperometry (CA) at −1.8 V vs Ag/AgCl for 1 h revealed stark differences in QAS performance depending on molecular structure. H12MS (*N*,*N*,*N*,*N*′,*N*′,*N*′-hexamethyl-1,12-dodecanediammonium methyl sulfate) was the most effective salt, suppressing hydrogen evolution from ∼0.76 to ∼0.11 mmol cm$^{-2}$ (an 85% decrease), even at concentrations as low as 1 μM. CA also showed that the monotonic increase in current over time for blank lead electrodes, which is due to corrosion and surface roughening, was also suppressed in the presence of QAS, underscoring their dual role as inhibitors of both HER and cathodic corrosion. Moreover, during the electrochemical hydrogenation of fumaric acid at −1.7 V vs Ag/AgCl, the addition of 1 mM H12MS enhanced the faradaic efficiency from 7.3% to 38.5% (a 5.3-fold increase) without affecting the yield of succinic acid. These findings highlight the effectiveness of QAS additives in tailoring the boundary layer to improve the efficiency and durability of electrochemical processes.

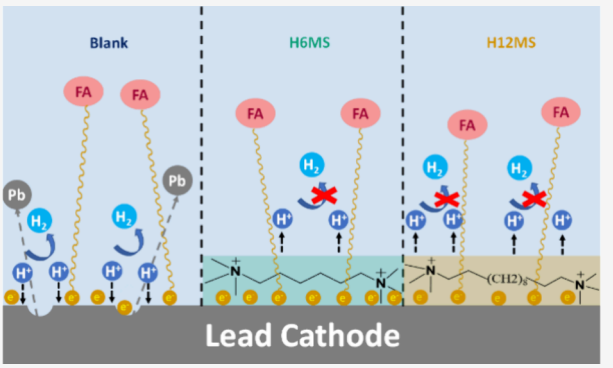


**KEYWORDS:** *Electrosynthesis, Quaternary ammonium, Hydrogen evolution reaction, Cathodic corrosion, Interface*



## INTRODUCTION

Electrochemical synthesis powered by renewable electricity offers a promising route to decarbonize the chemical industry.[1−4] Compared to traditional thermochemical processes that rely on fossil-derived heat to drive reactions, electrosynthesis enables clean redox transformations with lower waste generation and greenhouse gas emissions.[5] In particular, electro-organic synthesis has gained traction as a sustainable alternative for producing specialty chemicals and monomers,[6−8] eliminating the need for stoichiometric oxidants or reductants by using green electrons.[9−13] However, the deployment of these technologies at scale remains hampered by several challenges, especially for transformations in aqueous systems, where the hydrogen evolution reaction (HER) competes with the desired cathodic transformation.[14−16]

HER is a parasitic process that reduces faradaic efficiency (FE),[17,18] perturbs local pH, and contributes to cathodic corrosion of widely used electrodes such as lead,[19−21] tin,[22,23] and antimony.[24,25] It also promotes hydrogen bubble formation, increases local resistance, and leads to inhomogeneous current distribution, i.e., factors that limit the scalability and durability of electrolyzers.[26−28] These issues become more severe at high cathodic potentials and industrially relevant current densities, where HER can also degrade electrode surfaces via metal hydride formation,[29] hydrogen embrittlement, and mechanical damage caused by $H_2$ gas evolution.[30] These phenomena are particularly pronounced for lead cathodes, as reported in numerous studies.[21] At highly negative potentials, lead reacts with adsorbed hydrogen to form unstable lead hydride ($PbH_2$) species,[19] which induce brittleness in the metal, promote mechanical degradation, and facilitate the leaching of lead into the electrolyte. These effects are exacerbated by lead's relatively low shear strength[31]

Received: September 13, 2025
Revised: November 17, 2025
Accepted: November 20, 2025
Published: December 13, 2025

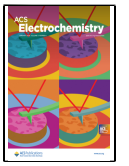

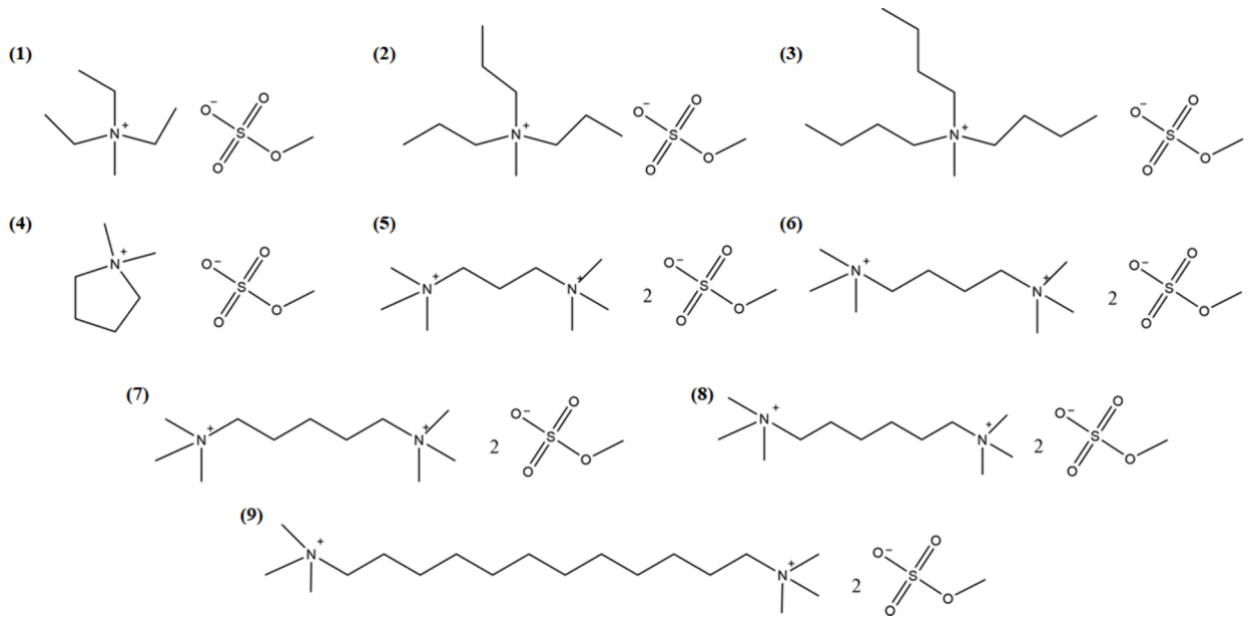


**Figure 1.** Molecular structures of the monomeric and dimeric quaternary ammonium salt (QAS) compounds **1**−**9** with different alkyl chain lengths and ammonium charge centers.

and poor mechanical stability[32] compared to other metals, making it especially susceptible to deformation under HER-induced stress. Given the toxicity of lead and its environmental implications,[33] new strategies to suppress its cathodic corrosion must be developed.

Mitigating HER without hindering productive organic reductions is therefore critical for advancing aqueous electrosynthesis. Several studies have explored the effect of electrolyte composition, especially the role of cations, on interfacial reactivity, but the results remain ambiguous. Monovalent inorganic cations like $Na^+$ and $K^+$ can accelerate HER and corrosion.[21,34−36] In contrast, quaternary ammonium salts (QAS) were used in the industrial electrodimerization of acrylonitrile to adiponitrile developed by Baizer,[37,38] where they were shown to inhibit HER and enhance both selectivity and FE. Surprisingly, QAS remain relatively understudied, although thousands of quaternary ammonium compounds with different molecular structures and charges are synthetically accessible, and theoretical studies predict their stability across a broad range of applied potentials.[38−40] This diversity highlights the need to systematically revisit their role in electrosynthesis and evaluate their potential for improving electrochemical manufacturing.

In this study, we explore how monomeric and dimeric QAS additives enhance the selectivity and stability of electrochemical reductions by modulating HER and cathodic corrosion at lead electrodes under acidic conditions (pH 1), where HER is typically pronounced. We hypothesized that QAS could favor electro-organic hydrogenation reactions over HER and corrosion by leveraging the mechanistic distinction between outer-sphere organic reductions and surface-mediated HER. Under operating conditions, the negatively charged cathode attracts QAS, which electrostatically self-assemble near the surface to form a barrier that hinders $H_3O^+$ diffusion, thereby reducing the rate of HER,[41,42] and cathodic corrosion[43−45] while still allowing electron transfer into the solution. This enables electrohydrogenations to proceed through solution-phase electron and proton transfer pathways.

To test this hypothesis, we first studied the HER and corrosion of lead cathodes under various reaction parameters using nine different QAS. Using the most promising inhibitor and reaction conditions, we then evaluated the performance and stability of lead electrodes during the electrochemical hydrogenation of fumaric acid, a representative organic substrate. In the presence of QAS, HER was suppressed by as much as 85%, with a cathodic shift in HER onset potential of nearly 200 mV. The faradaic efficiency for fumaric acid hydrogenation increased nearly fivefold from 7.4% to 38.5% without any loss in reaction rate, indicating selective HER suppression and mitigation of HER-induced corrosion. These results establish QAS as promising dual-function additives for improving the efficiency and durability of aqueous electrosynthetic systems.

## EXPERIMENTAL SECTION

**Synthesis of QAS.** Quaternary ammonium salts (QAS) were synthesized by treating tertiary amines with dimethyl sulfate. The tertiary amines were either commercially available or synthesized via Eschweiler-Clarke methylation of commercially available primary amines: triethylamine (Thermo Fisher Scientific, 99%), tripropylamine (Sigma-Aldrich, >98%), 1-methylpyrrolidine (Acros Organics, 98%), *N,N,N′,N′*-tetramethyl-1,3-propandiamine (Acros Organics, 99%), *N,N,N′,N′*-tetramethyl-1,6-hexanediamine (TCI, >98%), 1,4-diaminobutane (Merck Millipore, 99%), 1,5-diaminopentane (TCI, >98%), 1,12-diaminododecane (Sigma-Aldrich, 98%).[46] Formaldehyde (Carl Roth, 37%) and formic acid (Carl Roth, >98%) were used as general methylation reagents. All tertiary amines were purified by careful distillation prior to use. To prepare the QAS (compounds **1-9** in Figure 1), the tertiary amines were reacted with dimethyl sulfate (Acros Organics, 99%) in distilled tetrahydrofuran (technical grade). In a typical procedure, the amine precursor (0.1-0.4 mol) was dissolved in 100 mL of tetrahydrofuran. Dimethyl sulfate (1.05 equiv per amine functionality) was added dropwise over 30 min, maintaining the reaction temperature below 50 °C. The


https://doi.org/10.1021/acselectrochem.5c00398
ACS Electrochem. 2026, 2, 175−187

reaction mixture was stirred for 18 h at room temperature, and the solvent was removed under vacuum. The crude product was further purified by high vacuum drying (<0.01 mbar) at 50 °C for 12 h. The resulting QAS were colorless, semisolid materials of sufficient purity for further use. Compound 3 was provided by BASF SE (Ludwigshafen, Germany).

**Preparation of Lead Coupons.** Lead foil (99.99+%) was purchased from Sigma-Aldrich and cut into 1 cm x 3 cm x 1.05 mm coupons. The coupons were manually polished with 600- and 2000-grit sandpaper and dry-wiped with Kimwipes to remove any residual lead dust. Insulating tape was applied to both sides of the coupon, leaving an exposed area of 1 $cm^2$ on each side. The total active surface area, including all sides, was approximately 2.3 $cm^2$.

**Electrochemical Analysis for Corrosion.** Electrochemical measurements were conducted to evaluate the behavior and corrosion characteristics of lead coupons in 0.1 M $H_2SO_4$ (Sigma-Aldrich, research grade). A combination of techniques, including open circuit voltammetry (OCV), electrochemical impedance spectroscopy (EIS), and linear sweep voltammetry (LSV), was employed to characterize the baseline electrochemical behavior of the system. Additionally, chronoamperometry (CA), cyclic voltammetry (CV), and chronopotentiometry (CP) were used to study the corrosion dynamics of lead under various conditions.

All experiments were conducted using a single-compartment, three-electrode setup. Lead coupons served as the working electrode, a platinum coil as the counter electrode, and a saturated Ag/AgCl as the reference electrode (in 4 M KCl, Pine Research Instrumentation). Electrolyte solutions were freshly prepared prior to each experiment by dissolving varying concentrations of QAS (1, 10, 100, and 1000 $\mu$M) into 100 mL of 0.1 M $H_2SO_4$.

Electrochemical measurements were performed using a BioLogic VSP-300 potentiostat controlled via EC-Lab software (BioLogic, Claix, France). Prior to each measurement, the electrolyte was purged with argon gas for 15 min to remove dissolved oxygen, and an argon blanket was maintained throughout the experiment to ensure inert conditions.

OCV measurements were recorded for 30 min to allow the system to stabilize. EIS was then performed across a frequency range of 0.1 MHz to 0.1 Hz with an AC amplitude of 10 mV at the open circuit potential. LSVs were acquired from the OCP to −2.0 V vs Ag/AgCl at a scan rate of 50 mV $s^{-1}$. To analyze corrosion behavior, CA was conducted at −1.8 V for 1 h, followed by five CV cycles at 5 mV $s^{-1}$, and CP at a constant current of -100 mA, all under an argon atmosphere.

**Scanning Electron Microscopy.** Scanning electron microscopy (SEM) and energy-dispersive X-ray spectroscopy (EDS) were performed using a FEI Quanta 250 field-emission microscope equipped with an Oxford Aztec EDS detector. SEM images of polished lead coupons were recorded prior to each experiment, and the axial position of imaged areas was noted for subsequent analysis. The lead coupons were then subjected to chronoamperometry (CA) at −1.8 V vs Ag/AgCl in 0.1 M $H_2SO_4$ for 1 h, both in the absence and presence of 1 mM H12MS. The corroded coupons were lightly wiped to remove residual acid on the surface and dried using a gentle air stream. SEM images of the corroded coupons were recorded at the same axial positions to assess changes in surface morphology. EDS spectra were recorded from selected regions to determine the local and average elemental compositions.

**Electrochemical Analysis of Fumaric Acid Hydrogenation.** Cyclic voltammetry (CV) and linear sweep voltammetry (LSV) were conducted using a three-electrode system equipped with a lead rotating disk electrode (RDE, Pine Research) as the working electrode, a platinum coil as the counter electrode, and a saturated Ag/AgCl reference electrode (4 M KCl). All electrochemical measurements were carried out using a BioLogic VSP-300 potentiostat (BioLogic, Claix, France).

Prior to each experiment, the electrolyte solution was purged with argon gas for 15 min to remove dissolved oxygen, and an argon atmosphere was maintained throughout the experiment to ensure inert conditions. The RDE rotation speed was set to 1600 rpm for CV using an MSR rotator (Pine Research Instrumentation), and varied between 100 and 2500 rpm to analyze the kinetic current response and determine mass transport effects. A scan rate of 50 mV $s^{-1}$ was used for all voltammetry experiments. The electrolyte solutions were freshly prepared before each run by dissolving 1 g $L^{-1}$ of fumaric acid in 100 mL of 0.1 M $H_2SO_4$, with and without the addition of 1 mM QAS.

**Bulk Electrolysis.** Bulk electrolysis was performed in a single-compartment microflow cell reactor (ElectroCell, Amherst, NY), equipped with a lead plate as the working electrode, a platinized titania counter electrode, and a saturated Ag/AgCl reference electrode. The working and counter electrodes were separated by a PTFE spacer, establishing an inter-electrode gap of 3.6 mm. The reference electrode was connected to the cell via an orifice through the PTFE spacer. EPDM rubber gaskets ensured leak-proof sealing and confined the exposed electrode area to 10 $cm^2$. A PTFE mesh was inserted in the spacer to promote turbulence and enhance mass transfer. CA was carried out at potentials between −1.4 V and −1.8 V vs Ag/AgCl for 4 h using a BioLogic SP-150e potentiostat (BioLogic, Claix, France).

Electrolyte solutions were freshly prepared before each experiment by dissolving 4 g $L^{-1}$ of fumaric acid in 100 mL of 0.1 M $H_2SO_4$, with and without 1 mM QAS. The solution was continuously circulated through the reactor at a flow rate of 180 mL $min^{-1}$ using a Fisherbrand GP1000 peristaltic pump (Thermo Fisher Scientific).

Aliquots of 600 $\mu$L were sampled from the reactor at 30, 60, 120, 180, and 240 min for product analysis.

**Product Analysis.** Product identification and quantification were performed using proton nuclear magnetic resonance ($^1$H NMR) spectroscopy on a Bruker AVIII 600 MHz spectrometer. Each aliquot was first dried under airflow, and the residue was redissolved in deuterium oxide ($D_2O$) containing 1 g $L^{-1}$ of dimethyl malonic acid as an internal standard. The mass of the dried residue and the reconstituted solution were recorded. Quantification was carried out by integrating the relevant proton signals and normalizing against the internal standard. Conversion and selectivity were subsequently calculated using the integrated peak areas and corresponding weight fractions.

## RESULTS AND DISCUSSION

**Performance of the Synthesized QAS.** To evaluate the inhibitory performance of quaternary ammonium salts (QAS), a series of nine compounds were synthesized with systematically varied alkyl chain lengths and charge types (monomers and dimers) to probe the influence of molecular structure on HER suppression efficiency (Figure 1).


https://doi.org/10.1021/acselectrochem.5c00398
ACS Electrochem. 2026, 2, 175−187

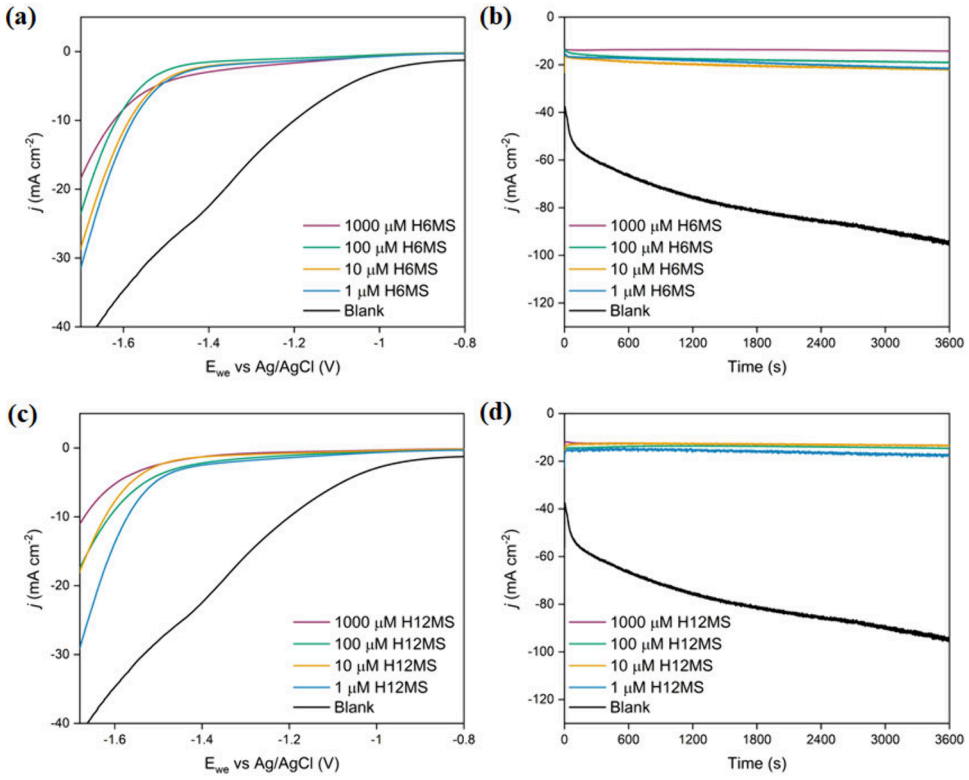


**Figure 2.** Performance of lead coupons in 0.1 M $H_2SO_4$ for various QAS concentrations. LSV: (a) H6MS and (c) H12MS; CA: (b) H6MS and (d) H12MS.

**Table 1. HER Onset Potential (vs Ag/AgCl) and Estimated $H_2$ Evolution of the Lead Coupons in the Presence of 1 mM QAS, Calculated from LSV and CA, Respectively**

| QAS | HER Onset (V) | ΔOnset (V) | Charge Density (C $cm^{-2}$) | Estimated $H_2$ (mmol $cm^{-2}$) | Suppression Efficiency (%) |
|---|---|---|---|---|---|
| 0.1 M $H_2SO_4$ (Blank) | −0.94 | | 146.54 | 0.76 | |
| Sample 1 | −1.10 | 0.16 | 87.48 | 0.46 | 40.3 |
| Sample 2 | −1.21 | 0.27 | 59.24 | 0.30 | 59.6 |
| Sample 3 | −1.52 | 0.58 | 44.33 | 0.23 | 69.8 |
| Sample 4 | −1.24 | 0.30 | 82.34 | 0.42 | 43.8 |
| Sample 5 | −1.56 | 0.62 | 62.75 | 0.32 | 57.2 |
| Sample 6 | −1.60 | 0.66 | 56.75 | 0.29 | 61.3 |
| Sample 7 | −1.62 | 0.68 | 51.08 | 0.26 | 65.1 |
| Sample 8 (H6MS) | −1.67 | **0.73** | 27.56 | 0.14 | **81.2** |
| Sample 9 (H12MS) | −1.71 | **0.77** | 21.13 | 0.11 | **85.3** |

Linear sweep voltammetry (LSV) was used to determine shifts in the onset potential of HER in the presence of the various QAS. In the blank electrolyte (without QAS), the onset of HER for the lead coupon was observed at approximately −0.94 V vs Ag/AgCl (Figure 2a), which deviates from values typically reported in the literature (−1.38 V vs Ag/AgCl).[47] This positive shift is attributed to the presence of a native lead oxide film, which remains even after polishing and is known to promote an earlier HER onset.[48] The addition of QAS at a concentration of 1 mM induced cathodic shifts in the HER onset potential (Table 1), thereby broadening the electrochemical window for productive reductions without HER interference.[49] The most significant shifts were recorded for QAS **8** and **9** (H6MS and H12MS, labeled based on the carbon chain length between quaternary ammoniums), with negative shifts of 0.73 and 0.77 V, respectively (Figures 2a,c). As the carbon chain length increased, both mono- and dicationic QAS exhibited greater HER suppression (Table 1). This trend likely reflects enhanced hydrophobic interactions and more effective interfacial structuring with longer alkyl chains, in particular in the case of dicationic QAS. Overall, the findings indicate that long-chain dicationic QAS are especially effective in repelling hydronium ions from the lead surface. Interestingly, the effectiveness of H6MS and H12MS remained pronounced even at concentrations as low as 1 $\mu$M. Additionally, the absence of current before the HER onset indicates that these QAS also mitigate HER for lead oxide surfaces.

In the absence of QAS, chronoamperometry (CA) revealed a monotonic increase in current over time (Figure 2b), attributed to the corrosion-driven roughening of the lead surface and the formation of new electrochemically-active surface area that promotes further HER.[34,50] In contrast, the currents were significantly lower and more stable in the presence of H6MS and H12MS (Figures 2b,d), indicating


https://doi.org/10.1021/acselectrochem.5c00398
ACS Electrochem. 2026, 2, 175−187

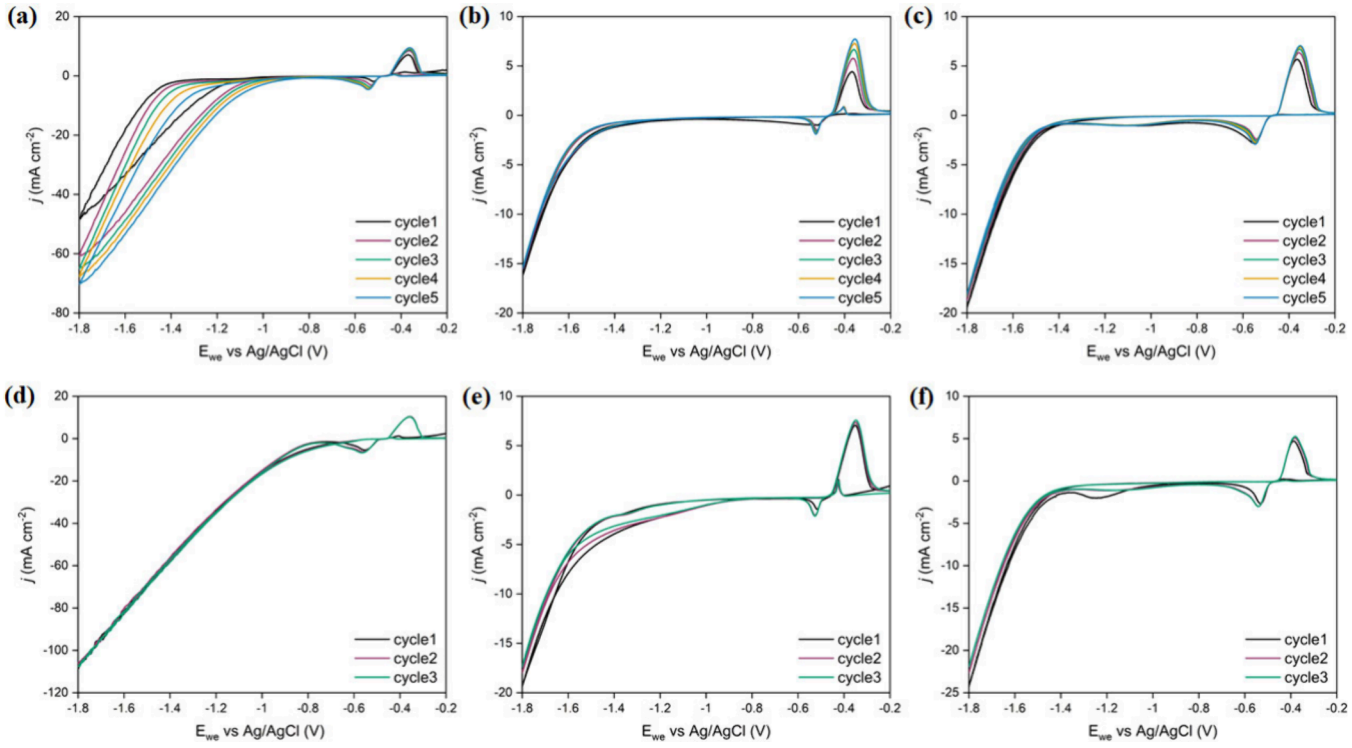


**Figure 3.** CV of lead coupons at a scan rate of 5 mV $s^{-1}$ in 0.1 M $H_2SO_4$: (a) blank, (b) 1 mM H12MS, (c) 1 mM H6MS, (d) blank after 1 h of HER (CA at −1.8 V vs Ag/AgCl), (e) 1 mM H12MS after 1 h of HER, and (f) 1 mM H6MS after 1 h of HER.

reduced corrosion and constant surface area during electrolysis.

The amount of evolved $H_2$ was calculated by integrating the current-time (I vs t) curves from CA measurements at a constant potential of −1.8 V vs Ag/AgCl for 1 h, using eq 1. Suppression efficiencies were then determined using eq 2, and these values are summarized in Table 1.

$$\text{Estimated } H_2 \text{ (mmol cm}^{-2}\text{)} = \frac{\text{Charge (C)} \times 1000}{2 \times 96500 \times \text{Surface area of coupon (cm}^2\text{)}} \quad (1)$$

$$\text{Suppression Efficiency (\%)} = \frac{\text{Est}H_2\text{(Blank)} - \text{Est}H_2\text{(QAS)}}{\text{Est}H_2\text{(Blank)}} \times 100 \quad (2)$$

Among all conditions tested, the highest estimated $H_2$ evolution was observed for the blank electrolyte (0.76 mmol $cm^{-2}$). In contrast, H6MS and H12MS yielded substantially lower values, 0.14 mmol $cm^{-2}$ and 0.11 mmol $cm^{-2}$, corresponding to suppression efficiencies of 81.2% and 85.3%, respectively. Furthermore, CA currents for H6MS and H12MS remained nearly constant even at concentrations as low as 1 $\mu$M. These results are consistent with the LSV data and confirm the superior performance of H6MS and H12MS in suppressing HER and stabilizing lead electrodes under acidic conditions. $H_2$ evolution was further quantified by online gas chromatography (GC) during CA at −1.8 V vs Ag/AgCl for 1 h in the absence and presence of QAS (Figure S1). The faradaic efficiencies for $H_2$ evolution are presented in Table S1 and range from 82 to 84%. Notably, hydrogen evolution was significantly suppressed in the presence of QAS compared to the blank, consistent with the suppression efficiencies calculated from LSV (Table 1).

**Corrosion Studies.** Cyclic voltammetry (CV) and chronopotentiometry (CP) were used to further evaluate the corrosion behavior of lead electrodes in the presence and absence of H6MS and H12MS. CVs were recorded at a slow scan rate of 5 mV $s^{-1}$ to provide sufficient time for HER to occur and to monitor the evolution of current responses over successive cycles. As shown in Figure 3a, the lead coupon in blank electrolyte exhibited increasing cathodic currents with each cycle, accompanied by a progressive shift in the HER onset potential toward more positive values. These changes indicate corrosion-induced surface roughening and chemical modification of the electrode. In contrast, Figures 3b-c show that both H6MS and H12MS stabilized the HER onset potential and suppressed current evolution across all cycles, indicating effective mitigation of HER-driven corrosion.

The peak observed at approximately −0.4 V vs Ag/AgCl in Figure 3 corresponds to the oxidation of lead to lead oxide (PbO). Integration of this anodic peak enabled quantification of the PbO formed, as shown in Figure S2. In the first CV cycle, the highest PbO formation was observed in the presence of H6MS, followed by the blank and H12MS. As lead oxidation is an electrochemical process, the extent of PbO formation reflects the rate of electron transfer between the lead surface and the bulk electrolyte. The greater oxide content in the H6MS case can be attributed to its lower charge-transfer resistance (vide infra). From cycle 1 to cycle 2, the blank exhibited a substantial increase in PbO formation, likely due to the oxidation of nascent lead surfaces generated during HER-driven corrosion. Overall, PbO formation increased progressively with each CV cycle for all cases, indicating that QAS species do not inhibit lead oxidation, in contrast to conventional corrosion inhibitors.


https://doi.org/10.1021/acselectrochem.5c00398
ACS Electrochem. 2026, 2, 175−187

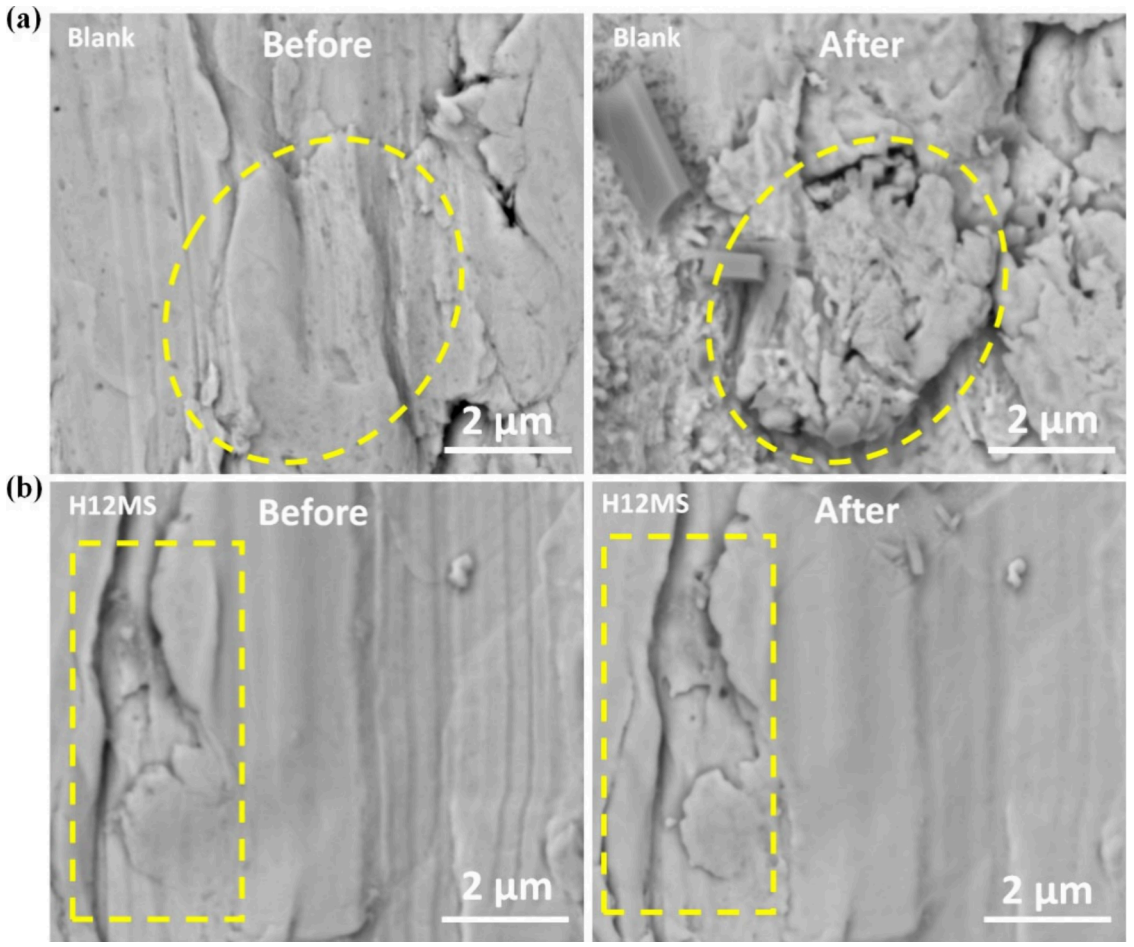


**Figure 4.** SEM images of lead coupons before and after corrosion under HER conditions (−1.8 V vs Ag/AgCl) for 1 h in 0.1 M $H_2SO_4$: (a) in the absence of QAS; (b) in the presence of 1 mM H12MS.

To further assess surface degradation, CVs were repeated after subjecting the lead electrodes to CA at −1.8 V vs Ag/AgCl for 1 h. As shown in Figure 3d, the post-CA CV in blank electrolyte displayed more than a two-fold increase in current compared to the pristine electrode. The HER onset potential also shifted positively, consistent with surface damage and accelerated corrosion. Notably, no further increase in current was observed with continued cycling, suggesting that the electrode had reached a passivated state, likely due to lead oxide formation. In contrast, Figures 3e-f show that lead electrodes in the presence of H6MS or H12MS exhibited no significant changes in CV profiles before and after 1 h of CA. These results confirm that QAS prevent corrosion and preserve the electrochemical properties of the lead surface.

Additional insight was obtained from CP at −100 mA (Figure S3). In the absence of QAS, the electrode potential drifted toward more positive values during electrolysis, consistent with the surface degradation observed in CV experiments. In contrast, in the presence of QAS, the potential remained stable over the entire 1 h duration, further demonstrating that QAS effectively protects the lead surface against HER-induced corrosion, even under aggressive electrochemical conditions. These results also demonstrate that H6MS and H12MS are electrochemically stable under these conditions, in good agreement with theoretical calculations that predicted their stability over a wide window of cathodic potentials.[38] Further, long-term CA experiments (Figure S4) showed that the current remained stable for at least 5 h in the presence of QAS, indicating their structural and electrochemical stability at high cathodic potentials.

**Surface Topology and Chemical Composition.** The surface topology of lead coupons was imaged before and after 1 h of HER at a potential of −1.8 V vs Ag/AgCl using scanning electron microscopy (SEM) to assess the protective effect of QAS additives. For consistent analysis, SEM images were acquired at the same surface location before and after the electrolysis by noting the x-y-z coordinates of the region of interest. As shown in Figure 4a, the lead surface exhibited extensive damage after 1 h of electrolysis in the blank electrolyte, including pronounced pitting and surface roughening indicative of severe cathodic corrosion. In contrast, the coupon exposed to 1 mM H12MS (Figure 4b) retained a relatively smooth and intact surface, confirming the effectiveness of QAS in mitigating HER-driven corrosion. Similar corrosion-induced etching and redeposition have been observed for metallic alloys in prior studies, but direct corrosion suppression using supporting electrolytes has not previously been demonstrated.[51]

Energy-dispersive X-ray spectroscopy (EDS) was used to quantify changes in surface composition before and after electrolysis, and the results are summarized in Table S2. A notable increase in oxygen content from 0.88 to 6.06 wt % was observed for coupons tested without QAS (blank), and from 0.91 to 4.41 wt % in the presence of 1 mM H12MS, indicating


https://doi.org/10.1021/acselectrochem.5c00398
ACS Electrochem. 2026, 2, 175−187

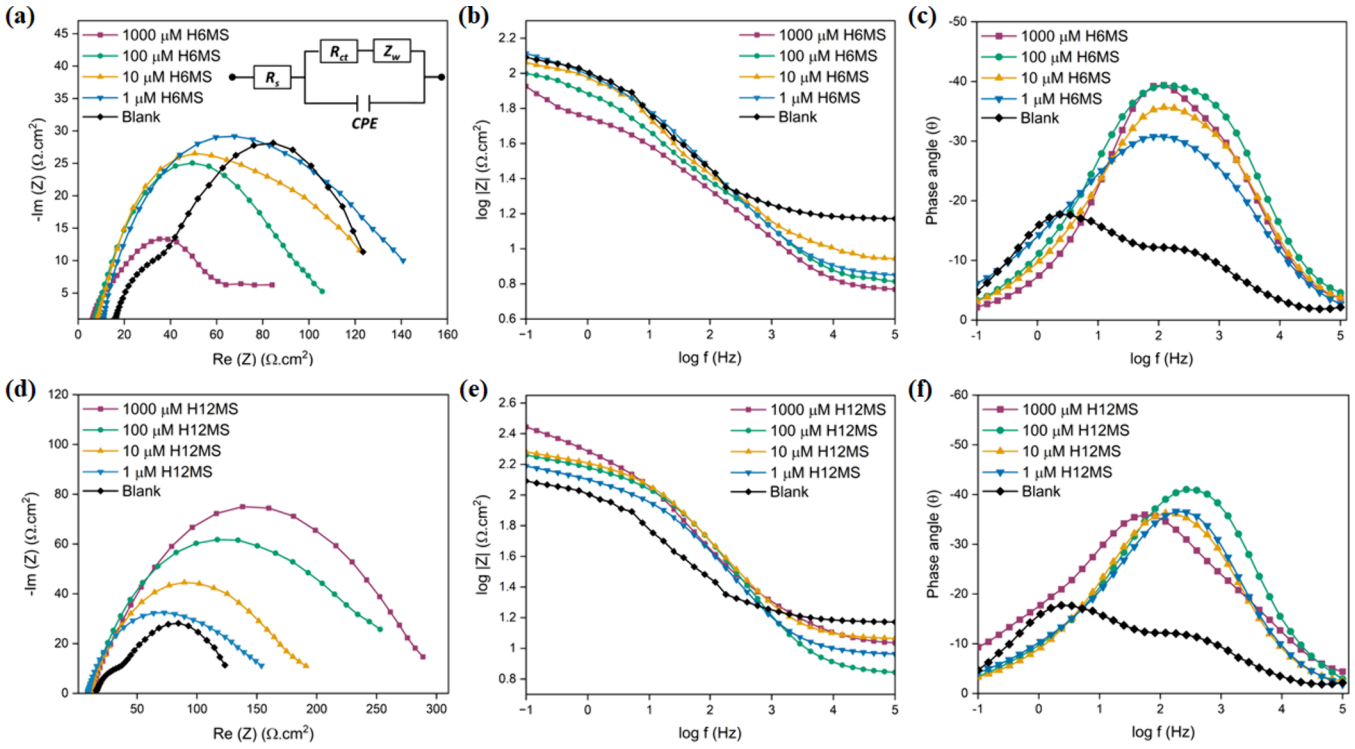


**Figure 5.** PEIS and Bode plots of lead coupons in 0.1 M $H_2SO_4$ at different concentrations of H6MS (a–c); H12MS (d–f).

partial surface oxidation. This is consistent with the CV profiles in Figure 3, which show an increase in the peak at −0.4 V vs Ag/AgCl corresponding to the lead oxide. Although Pourbaix diagrams predict that lead remains in its elemental state at pH 1 under these electrochemical conditions,[52] these results suggest the formation of an oxide layer. But, importantly, while both untreated and QAS-treated samples exhibit increased oxygen content, only the untreated sample shows clear signs of structural degradation. This indicates that QAS do not impede surface oxidation but prevent its progression to corrosive damage, as supported by the SEM data.

To complement the EDS analysis and specifically assess whether QAS species remain on the surface after electrolysis, the surface composition was further analyzed by X-ray photoelectron spectroscopy (XPS). This technique offers greater surface sensitivity and elemental resolution for light elements such as nitrogen (Figure S5). The survey and N 1s spectra of corroded and non-corroded lead coupons show no discernible nitrogen signals for any of the samples. This absence indicates that QAS molecules are not retained on the surface after depolarization and rinsing, consistent with adsorption driven primarily by electrostatic attraction under cathodic bias rather than chemisorption.

**Analysis of the Metal-Electrolyte Interface by Electrochemical Impedance Spectroscopy and Open-Circuit Voltammetry.** The electrochemical impedance of lead coupons in the presence of QAS was assessed using Nyquist plots, from which the charge transfer resistance ($R_{ct}$, Table S3) was calculated by fitting a Randles equivalent circuit. In contrast, the Nyquist plot for the blank electrolyte displayed two distinct semicircles, indicative of multiple interfacial processes with different time constants. This behavior likely arises from separate charge-transfer resistances associated with the lead surface and corrosion-induced surface transformations. A more complex equivalent circuit was therefore used for this case, as shown in Figure S6. For most QAS, $R_{ct}$ values were lower than that of the blank lead coupon, with the exception of H12MS. The reduced $R_{ct}$ values can be attributed to the ionic nature of QAS, which enhances conductivity at the solid-liquid interface and facilitates electron transfer from the lead cathode to the bulk electrolyte, thereby promoting the desired reduction reactions while repelling $H_3O^+$ ions. The higher $R_{ct}$ value for H12MS likely results from its longer non-conductive alkyl chain, which may form insulating regions that hinder charge transfer.

Nyquist, Bode magnitude, and phase angle plots for H6MS and H12MS at various concentrations are shown in Figure 5, and the corresponding $R_{ct}$ values are presented in Table 2. For H6MS, increasing the concentration leads to a decrease in low-frequency impedance (Figure 5b), consistent with enhanced charge transfer and improved double-layer conductivity

**Table 2. Charge Transfer Resistance ($R_{ct}$) Calculated from Nyquist Plots Obtained from EIS of Lead Coupons in the Presence of Varying Concentrations of H6MS and H12MS in 0.1 M $H_2SO_4$**

| QAS | $R_{ct}$ (Ω·cm²) |
|---|---|
| 0.1 M $H_2SO_4$ (Blank) | 149.27 |
| H6MS | |
| 1000 μM | 84.52 |
| 100 μM | 118.79 |
| 10 μM | 142.30 |
| 1 μM | 153.09 |
| H12MS | |
| 1000 μM | 236.67 |
| 100 μM | 213.21 |
| 10 μM | 164.50 |
| 1 μM | 111.66 |


https://doi.org/10.1021/acselectrochem.5c00398
ACS Electrochem. 2026, 2, 175−187

(Figure 5a). In contrast, H12MS shows increasing low-frequency impedance with increasing concentration (Figure 5e), consistent with reduced ionic conductivity due to its longer alkyl chain. The phase angle plots (Figures 5c,f) provide further insight. In the blank electrolyte, two distinct peaks and low overall phase angles are observed, indicative of overlapping processes such as charge transfer and corrosion-induced surface transformations. In contrast, the addition of QAS yields a single peak, implying that charge transfer across the double layer becomes the dominant process. In both cases, the maximum phase angle remains below 45°, consistent with the formation of an electrochemically active double layer.

Open circuit voltammetry measurements were conducted to determine the open circuit potential (OCP) of the lead working electrode in 0.1 M $H_2SO_4$ and to examine how it is affected by the addition of QAS (Figure S7). In the absence of QAS, the lead electrode exhibited a relatively negative OCP of −0.482 V vs Ag/AgCl, which favors the electrostatic accumulation of cationic QAS at the surface. Upon addition of H6MS or H12MS, the OCP shifted positively, with the magnitude of the shift increasing with QAS concentration, consistent with the formation of a self-assembled cationic layer near the electrode. To validate that this behavior is governed by surface charge, we performed analogous OCP measurements on copper and platinum, which exhibit more positive OCPs (Figure S8). In parallel, we experimentally determined the potential of zero total charge (PZTC) for Pb and Cu by measuring the double-layer capacitance as a function of applied potential using EIS (Figure S9). The results confirmed that both OCP and PZTC are negative for lead and positive for copper, indicating consistency between these two descriptors under our conditions.

No shift in HER onset potential was observed upon QAS addition for Cu and Pt electrodes (Figure S10), confirming that QAS adsorption is governed by the interfacial potential: QAS interact with negatively charged Pb surfaces, but not with the more positively charged Cu or Pt surfaces. To further probe this interaction, we performed CA at −1.0 and −1.8 V vs Ag/AgCl on platinum and lead electrodes, respectively, corresponding to applied potentials more negative than the PZTC of the metal. CA was allowed to proceed for 15-20 min in 0.1 M $H_2SO_4$, after which 1 mM QAS was introduced to monitor changes in current response (Figure S11). For Pb, the addition of QAS caused a sharp decrease in current, which then remained low for the remainder of the experiment, indicating effective HER inhibition. In contrast, the current for Pt remained essentially unchanged upon QAS addition, indicating that QAS had no measurable effect.

This observation contrasts with the findings of Resasco and co-workers, who reported that cationic species accumulate at cathodes held at potentials more negative than the PZTC and modulate reaction rates in alkaline media.[53] Under our acidic conditions, however, the Gibbs free energy of proton adsorption on Pt and Cu is significantly more favorable than that of QAS adsorption, preventing QAS from effectively competing with $H_3O^+$ at the interface. For Pb, which has a high hydrogen overpotential and positive Gibbs free energy for hydrogen binding, the opposite trend allows QAS to outcompete proton adsorption and effectively suppress HER.

Finally, it is worth noting that the OCP values of lead (Figure S7) remained within ±85 mV of the blank upon QAS addition at various concentrations.[54] This modest variation suggests that QAS exhibits mixed-mode inhibition by protecting both anodic and cathodic sites.[55]

**Electrochemical Hydrogenation of Fumaric Acid.** Although QAS exhibited strong performance in suppressing HER and mitigating HER-driven cathodic corrosion on lead cathodes, a key objective in electrosynthesis is to enhance the rate and faradaic efficiency for the desired transformations. To evaluate the influence of QAS on electro-organic synthesis, the electrochemical hydrogenation (ECH) of fumaric acid to succinic acid was selected as a model reaction. This transformation was carried out in 0.1 M $H_2SO_4$ using a lead working electrode. Previous studies have established that the ECH of fumaric acid on lead proceeds via proton-coupled electron transfer (PCET) in the bulk electrolyte, rather than through direct surface-mediated hydrogenation, similar to many non-catalytic electro-organic synthesis reactions.[47] Given that QAS are hypothesized to self-assemble near the electrode and suppress surface-mediated HER, the cations were not expected to significantly interfere with outer-sphere ECH processes occurring in solution.

Cyclic voltammetry results in Figure 6 supported this hypothesis. In the presence of 1 g $L^{-1}$ fumaric acid, two

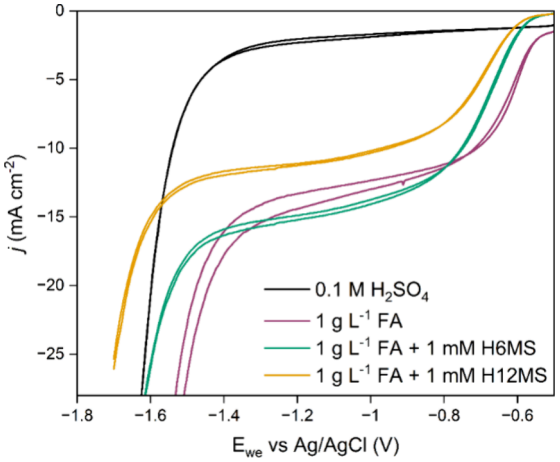


**Figure 6.** Cyclic voltammograms of lead RDE in the presence of 1 g $L^{-1}$ fumaric acid with and without 1 mM H6MS or H12MS.

distinct onset potentials were observed: onset (I) around −0.57 V vs Ag/AgCl assigned to the ECH of fumaric acid, and onset (II) around −1.38 V vs Ag/AgCl corresponding to the onset of HER.[47] No significant change was observed in onset (I) upon addition of 1 mM H6MS, while H12MS produced a modest cathodic shift of ∼30 mV. In contrast, onset (II) shifted substantially toward more negative potentials, by approximately 140 mV for H6MS and 200 mV for H12MS. This strong shift in HER onset indicated that QAS created additional kinetic barriers for HER while exerting only minimal influence on the hydrogenation of fumaric acid.

To further assess the impact of QAS on ECH kinetics, linear sweep voltammetry was performed at various rotation speeds, and Koutecký-Levich plots were constructed to determine kinetic current densities (Figure 7) using the following eq 3.[56]

$$\frac{1}{i_L} = \frac{1}{i_K} + \frac{1}{B_L \omega^{0.5}} \quad (3)$$

The extracted kinetic current values were highest for 1 mM H6MS, followed by the blank electrolyte, and lowest for 1 mM


https://doi.org/10.1021/acselectrochem.5c00398
ACS Electrochem. 2026, 2, 175−187

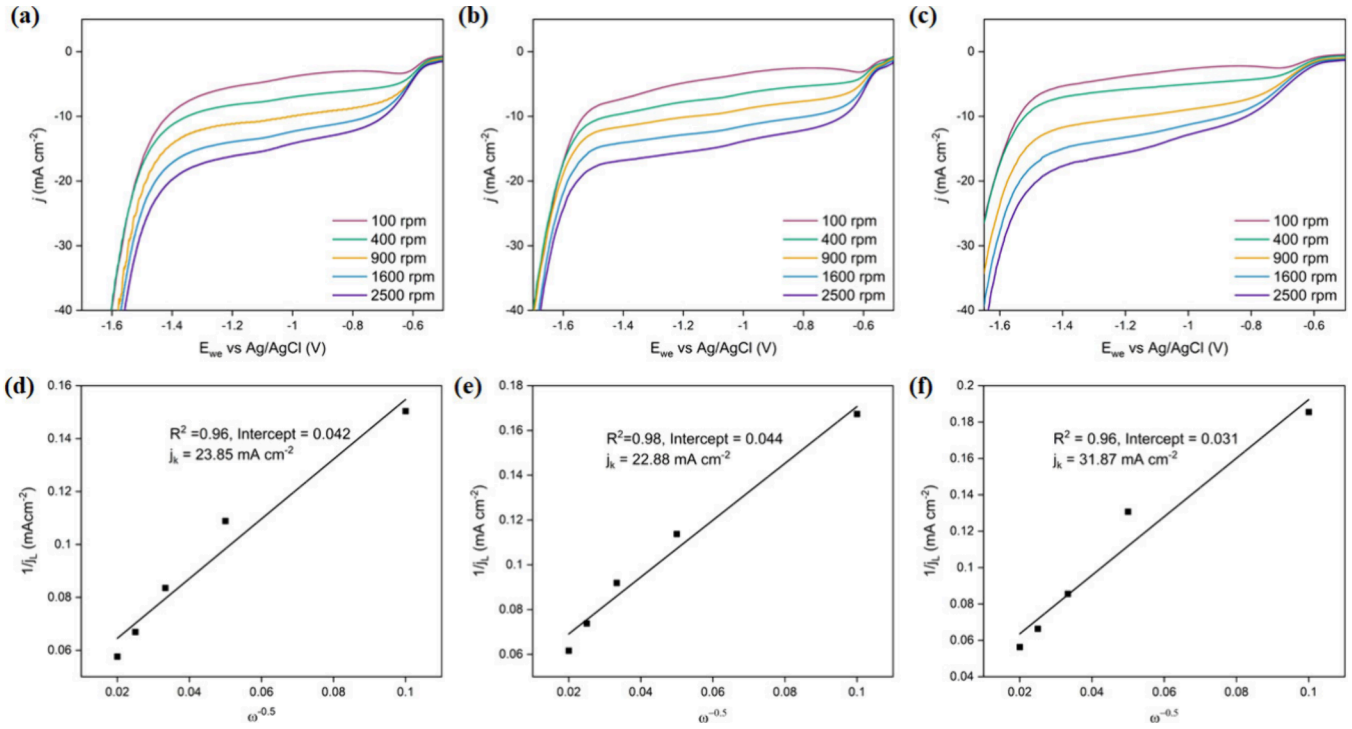


**Figure 7.** LSV curves for lead RDE in 1 g $L^{-1}$ fumaric acid at various rotation speeds and corresponding Koutecký-Levich plots for (a, d) Blank, (b, e) 1 mM H6MS, and (c, f) 1 mM H12MS.

H12MS (Figures 7d-f). Since the kinetic current is directly proportional to the reaction rate, these results suggested that the rate of fumaric acid hydrogenation was enhanced in the presence of H6MS. This enhancement was consistent with the lower charge transfer resistance ($R_{ct}$) of H6MS, which facilitated efficient electron transport from the lead electrode to the bulk electrolyte. Conversely, the reduced ECH rate observed with H12MS was likely due to its higher $R_{ct}$, which hindered electron transfer and limited hydrogenation efficiency relative to the blank.

**Bulk Electrolysis.** Bulk electrolysis was performed to evaluate the effect of QAS on the yield and faradaic efficiency of fumaric acid reduction, as well as to determine the optimal potential for conducting the ECH of fumaric acid. In all cases, succinic acid was obtained as the sole organic product, corresponding to 100% selectivity. Figures 8a-c show that as the applied potential was increased from −1.5 to −1.7 V vs Ag/AgCl, the HER rate increased, as indicated by broader current bands and higher current magnitudes in the I vs t curves. Under these conditions, a pronounced time-dependent increase in current was observed for the blank electrolyte, indicating the onset and progression of cathodic corrosion. In contrast, the presence of QAS significantly attenuated this current rise, indicating effective suppression of HER and the associated corrosion. Interestingly, in Figure 8c, while a gradual increase in current was observed in the presence of 1 mM H6MS at −1.7 V, this behavior was not seen with 1 mM H12MS, suggesting that H12MS offers superior HER suppression compared to H6MS under these conditions.

The succinic acid yields and faradaic efficiencies obtained at different potentials, with and without QAS, were calculated using Equations 4-7) and are summarized in Figures 8d-f. In general, slightly lower yields were recorded in the presence of QAS compared to the blank, with the exception of 1 mM H6MS at −1.7 V vs Ag/AgCl (Figure 8f). The higher yields observed in the blank electrolyte at −1.5 and −1.6 V (Figures 8d,e) are likely due to HER-induced surface roughening, which increased the electrochemically active surface area. This roughened surface facilitates additional charge transfer, enhancing the conversion of fumaric acid to succinic acid. Conversely, the lower yields observed with H12MS may reflect slower electron transfer kinetics for the ECH process, consistent with the Koutecký-Levich analysis. Remarkably, at −1.7 V, 1 mM H6MS outperformed the blank, likely because HER consumed a greater fraction of the available electrons in the absence of QAS, thereby reducing conversion efficiency.

ECH reaction:

$$FA + 2H^+ + 2e^- \rightarrow SA \quad (4)$$

Parasitic HER reaction:

$$2H^+ + 2e^- \rightarrow H_2 \quad (5)$$

$$\text{Yield of SA (\%)} = \frac{\text{moles of SA formed}}{\text{initial moles of FA}} \times 100\% \quad (6)$$

$$\text{FE of SA (\%)} = \frac{\text{moles of SA} \times 2 \times 96{,}485}{\text{Charge}} \times 100\% \quad (7)$$

While product yields were comparable across conditions, QAS additives had a much more pronounced impact on faradaic efficiency. As shown in Figure 8g, at −1.5 V vs Ag/AgCl, where HER is minimal, initial FE values correlated with the intrinsic hydrogenation rate. Over time, however, HER-driven corrosion in the blank increased the total current and lowered FE relative to QAS-containing electrolytes. At more negative potentials (Figure 8h-i), where HER becomes more prominent, FE in the blank dropped substantially due to corrosion-induced formation of a new electrode surface, which further promoted HER. Under these conditions, H12MS


https://doi.org/10.1021/acselectrochem.5c00398
ACS Electrochem. 2026, 2, 175−187

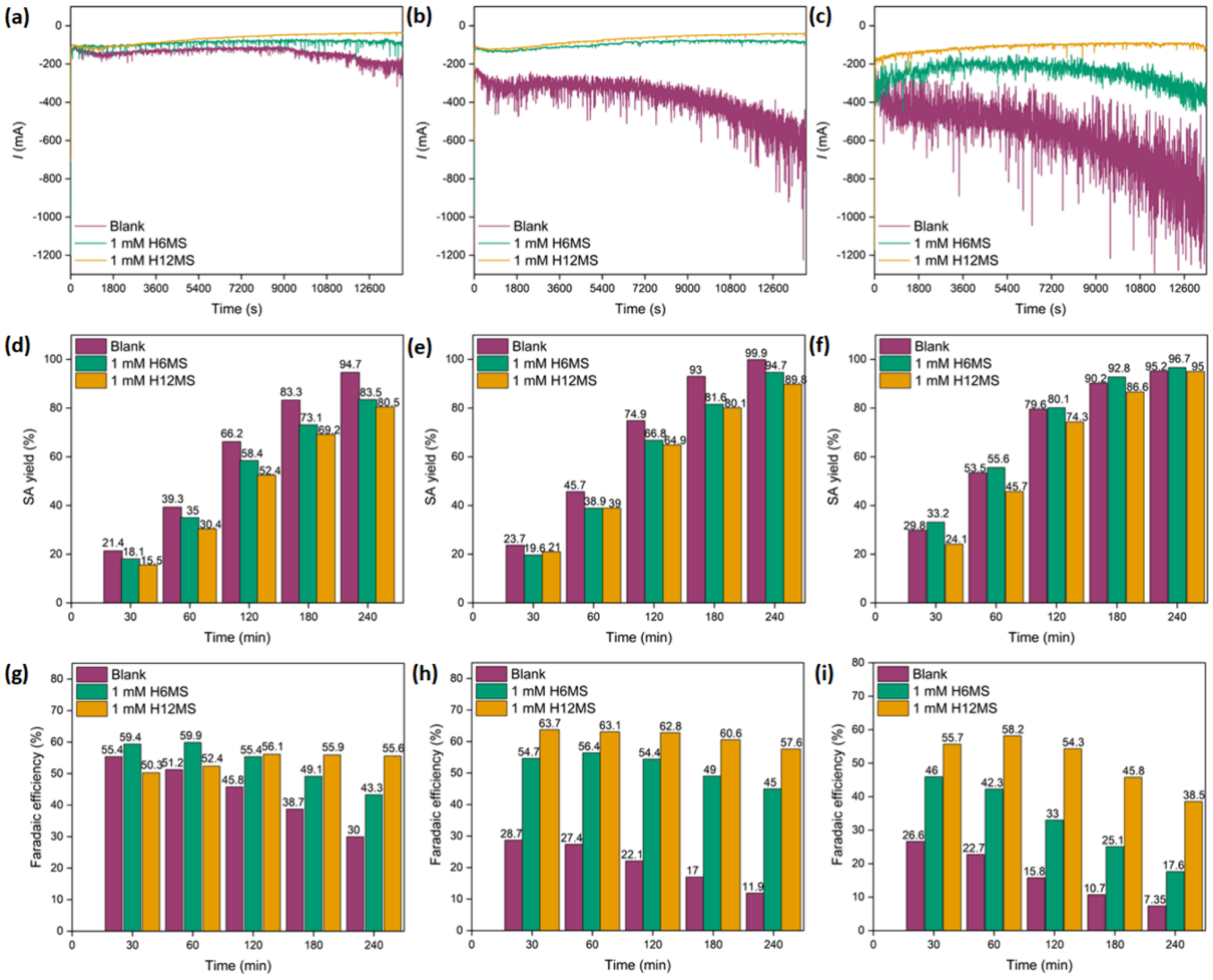


**Figure 8.** ECH of 4 g $L^{-1}$ fumaric acid at pH 1 on lead cathode by bulk electrolysis in the absence and presence of 1 mM H6MS or H12MS. (a–c) Chronoamperometry performed at −1.5, −1.6, and −1.7 V vs Ag/AgCl, respectively; (d–f) succinic acid yield at various times, (g–i) faradaic efficiency at these different applied potentials.

consistently maintained higher FE values than H6MS, demonstrating superior HER suppression and corrosion protection. This is especially evident from Figure 8i, where FE remained relatively stable for H12MS but declined sharply for H6MS.

**Role of QAS in Structuring the Electrode-Electrolyte Microenvironment.** The addition of QAS to the electrolyte induces substantial changes in the interfacial microenvironment at the negatively charged lead cathode. Under cathodic conditions, cationic QAS electrostatically accumulate near the electrode surface, forming a self-assembled layer that populates the outer Helmholtz plane (OHP) without undergoing chemisorption.[57,58] XPS analysis (Figure S5) confirms the absence of strongly bound nitrogen-containing species on the surface, indicating that QAS interactions are primarily electrostatic in nature. This interpretation is consistent with prior operando infrared spectroscopy studies by Mathison et al., who showed that tetraalkylammonium ions enrich the near-electrode region but do not bind directly to the electrode surface.[41]

Beyond their electrostatic accumulation, the alkyl chains of QAS impart hydrophobic character to the interfacial region.[57,59] This dual electrostatic-hydrophobic barrier impedes the approach and solvation of hydronium ions ($H_3O^+$), thereby suppressing the hydrogen evolution reaction (HER) through both kinetic and mass transport limitations. As the length of the alkyl spacer increases from H6MS to H12MS, the resulting interface becomes increasingly hydrophobic, further preventing proton access and water adsorption onto the cathode surface. This trend is consistent with the enhanced HER suppression observed experimentally for H12MS.

Importantly, while QAS hinder proton access to the surface, they do not impede outer-sphere electron transfer. Enhancements in faradaic efficiency for ECH were achieved because electro-organic hydrogenations such as the reduction of fumaric acid proceed predominantly via solution-phase proton-coupled electron transfer (PCET) mechanisms, which can occur within the diffuse layer or bulk solution.[47] Thus, QAS selectively suppress HER, a surface-mediated reaction, without compromising desired transformations that occur in solution.


https://doi.org/10.1021/acselectrochem.5c00398
ACS Electrochem. 2026, 2, 175−187

EIS further reveals the influence of QAS on charge transfer resistance ($R_{ct}$). For short-chain mono- and dicationic QAS (e.g., H6MS), $R_{ct}$ values are lower than for the blank electrolyte, indicating improved double-layer conductivity (Tables 2 and S3). In contrast, H12MS exhibits a higher $R_{ct}$, likely due to its longer alkyl chains forming a more resistive, non-conductive interfacial region. This increased $R_{ct}$ is correlated with slower kinetics in the electrochemical hydrogenation of fumaric acid (vide supra), highlighting how interfacial structuring by QAS modulates both HER suppression and organic reaction rates.

## CONCLUSION

In electro-organic synthesis, the hydrogen evolution reaction is a parasitic side process that reduces the faradaic efficiency and promotes the cathodic corrosion of lead electrodes. To address these limitations, we introduced quaternary ammonium salts (QAS) to limit proton diffusion to the electrode surface. Among the nine compounds synthesized, H6MS and H12MS exhibited exceptional performance in HER inhibition and corrosion mitigation. Electrochemical characterizations (LSV, CA, CV, and CP) confirmed that corrosion of bare lead electrodes leads to a monotonic rise in current over time due to the generation of new active sites. In contrast, the current remained low and stable in the presence of QAS, indicating that HER and corrosion were effectively inhibited. These observations were corroborated by SEM imaging, which showed severe surface degradation on bare lead but minimal morphological changes in the presence of QAS after electrolysis.

The impact of QAS on electrosynthetic transformations was further evaluated using the ECH of fumaric acid as a model reaction involving outer-sphere electron and proton transfers, representative of a broad class of electro-organic reactions. Koutecký−Levich analysis indicated that QAS had minimal effect on ECH kinetics. However, bulk electrolysis revealed that HER and cathodic corrosion intensified at more negative potentials, drastically reducing faradaic efficiency. The addition of QAS enhanced FE by over fivefold without compromising product yield, underscoring their ability to selectively suppress HER while preserving the desired transformations.

Overall, QAS additives such as H12MS and H6MS offer a promising strategy to enhance the efficiency and durability of aqueous electrosynthetic processes. By electrostatically accumulating near the cathode surface and establishing a hydrophobic barrier, these cations restructure the electrode-electrolyte microenvironment to selectively inhibit HER while preserving solution-phase electro-organic reactions. This dual function, simultaneously suppressing parasitic proton reduction and mitigating cathodic corrosion, opens new avenues for developing robust, tunable electrochemical systems tailored to sustainable chemical manufacturing.

## ASSOCIATED CONTENT

### Supporting Information

The Supporting Information is available free of charge at https://pubs.acs.org/doi/10.1021/acselectrochem.5c00398.

Amount of $H_2$ evolved over a lead cathode for 1 h in the presence and absence of QAS using GC, comparative lead oxide formation for lead electrodes in the absence and presence of QAS, CP at −100 mA in the presence and absence of 1 mM QAS, CA of lead coupon at −1.8 V vs Ag/AgCl in the presence of QAS for 12 h, XPS spectra of lead coupons before and after corrosion, equivalent circuit of blank lead coupon, OCV for lead coupons in the presence and absence of different concentrations of QAS, OCV of copper and platinum in blank electrolyte, PZC of lead and copper, CVs of copper and platinum in the presence of and absence of 1 mM QAS, CA of platinum and lead with 1 mM QAS introduced during the experiment, amount of $H_2$ evolved and FE for 1 h of CA at −1.8 V, elemental composition of lead coupons before and after corrosion, EIS of lead coupons in the presence and absence of 1 mM of various QASs (PDF)

## AUTHOR INFORMATION


### Corresponding Authors

**Jean-Philippe Tessonnier** − *Department of Chemical & Biological Engineering, Iowa State University, Ames, Iowa 50011, United States; Center for Biorenewable Chemicals (CBiRC), Ames, Iowa 50011, United States;* orcid.org/0000-0001-9035-634X; Email: tesso@iastate.edu

**Siegfried R. Waldvogel** − *Max-Planck-Institute for Chemical Energy Conversion, Department of Electrosynthesis, Mülheim an der Ruhr 45470, Germany;* orcid.org/0000-0002-7949-9638; Email: siegfried.waldvogel@cec.mpg.de

### Authors

**Achanta K. S. Koushik** − *Department of Chemical & Biological Engineering, Iowa State University, Ames, Iowa 50011, United States; Center for Biorenewable Chemicals (CBiRC), Ames, Iowa 50011, United States;* orcid.org/0009-0005-2718-0923

**Pietro Vannini** − *Department of Chemical & Biological Engineering, Iowa State University, Ames, Iowa 50011, United States;* orcid.org/0009-0009-7271-2617

**Eva Plut** − *Max-Planck-Institute for Chemical Energy Conversion, Department of Electrosynthesis, Mülheim an der Ruhr 45470, Germany;* orcid.org/0000-0002-2630-7284

**Wiebke Jansen** − *Max-Planck-Institute for Chemical Energy Conversion, Department of Electrosynthesis, Mülheim an der Ruhr 45470, Germany*

Complete contact information is available at: https://pubs.acs.org/10.1021/acselectrochem.5c00398


### Author Contributions

The manuscript was written through the contributions of all authors. All authors have given approval to the final version of the manuscript. Achanta K. S. Koushik: Conceptualization, Methodology, Investigation, Validation, Data Curation, Formal Analysis, Visualization, Writing−Original Draft, Writing−Review and Editing. Pietro Vannini: Investigation, Data Curation. Eva Plut: Data Curation, Writing−Original Draft. Wiebke Jansen: Data Curation, Writing−Original Draft. Siegfried R. Waldvogel: Conceptualization, Supervision, Funding Acquisition, Writing−Review and Editing. Jean-Philippe Tessonnier: Conceptualization, Visualization, Supervision, Project Administration, Funding Acquisition, Writing−Review and Editing.

### Notes

The authors declare no competing financial interest.



https://doi.org/10.1021/acselectrochem.5c00398
ACS Electrochem. 2026, 2, 175−187

## ■ ACKNOWLEDGMENTS

This material is based upon work supported by the National Science Foundation under Award No. 2140342 and the Deutsche Forschungsgemeinschaft (DFG) under Award Nos. Wa1276/27-1 and Wa1276/31-1.

## ■ REFERENCES

(1) Xia, R.; Overa, S.; Jiao, F. Emerging Electrochemical Processes to Decarbonize the Chemical Industry. *JACS Au* **2022**, *2* (5), 1054−1070.
(2) Baldea, M.; Endler, E. E.; Hale, E.; Maravelias, C. T.; Barolo, M.; Harjunkoski, I.; Mercangoz, M.; Shah, S. L.; Soroush, M.; Young, B. R.; et al. Transforming the Process Industries through Electrification: Challenges and Opportunities. *Industrial & Engineering Chemistry Research* **2025**, *64*, 16466.
(3) Chen, S. S.; Glezakou, V.-A.; Holewinski, A.; Lopez-Ruiz, J.; Tessonnier, J.-P. Advances in electrosynthesis for a greener chemical industry. *Green Chem.* **2024**, *26* (8), 4240−4241.
(4) Aviso, K. B. Decarbonizing the chemical industry through digital technologies. *Digital Chemical Engineering* **2025**, *16*, 100250.
(5) Zito, A. M.; Clarke, L. E.; Barlow, J. M.; Bím, D.; Zhang, Z.; Ripley, K. M.; Li, C. J.; Kummeth, A.; Leonard, M. E.; Alexandrova, A. N.; et al. Electrochemical Carbon Dioxide Capture and Concentration. *Chem. Rev.* **2023**, *123* (13), 8069−8098.
(6) Tian, C.; Dorakhan, R.; Wicks, J.; Chen, Z.; Choi, K.-S.; Singh, N.; Schaidle, J. A.; Holewinski, A.; Vojvodic, A.; Vlachos, D. G.; et al. Progress and roadmap for electro-privileged transformations of bio-derived molecules. *Nature Catalysis* **2024**, *7* (4), 350−360.
(7) Akhade, S. A.; Singh, N.; Gutiérrez, O. Y.; Lopez-Ruiz, J.; Wang, H.; Holladay, J. D.; Liu, Y.; Karkamkar, A.; Weber, R. S.; Padmaperuma, A. B.; et al. Electrocatalytic Hydrogenation of Biomass-Derived Organics: A Review. *Chem. Rev.* **2020**, *120* (20), 11370−11419.
(8) Dell'Anna, M. N.; Laureano, M.; Bateni, H.; Matthiesen, J. E.; Zaza, L.; Zembrzuski, M. P.; Paskach, T. J.; Tessonnier, J.-P. Electrochemical hydrogenation of bioprivileged cis,cis-muconic acid to trans-3-hexenedioic acid: from lab synthesis to bench-scale production and beyond. *Green Chem.* **2021**, *23* (17), 6456−6468.
(9) Panizza, M.; Cerisola, G. Direct And Mediated Anodic Oxidation of Organic Pollutants. *Chem. Rev.* **2009**, *109* (12), 6541−6569.
(10) Frontana-Uribe, B. A.; Little, R. D.; Ibanez, J. G.; Palma, A.; Vasquez-Medrano, R. Organic electrosynthesis: a promising green methodology in organic chemistry. *Green Chem.* **2010**, *12* (12), 2099−2119.
(11) Stephen, H. R.; Röckl, J. L. The Future of Electro-organic Synthesis in Drug Discovery and Early Development. *ACS Organic & Inorganic Au* **2024**, *4* (6), 571−578.
(12) Pollok, D.; Waldvogel, S. R. Electro-organic synthesis - a 21st century technique. *Chemical Science* **2020**, *11* (46), 12386−12400.
(13) Wiebe, A.; Gieshoff, T.; Möhle, S.; Rodrigo, E.; Zirbes, M.; Waldvogel, S. R. Electrifying Organic Synthesis. *Angew. Chem., Int. Ed.* **2018**, *57* (20), 5594−5619.
(14) Xia, R.; Tian, D.; Kattel, S.; Hasa, B.; Shin, H.; Ma, X.; Chen, J. G.; Jiao, F. Electrochemical reduction of acetonitrile to ethylamine. *Nat. Commun.* **2021**, *12* (1), 1949.
(15) Khalil, M.; Kadja, G. T. M.; Nugroho, F. A. A.; Sutanto, L. G.; Jiwanti, P. K.; Abdi, F. F.; Hussin, F.; Aroua, M. K. Suppressing the competing hydrogen evolution reaction in CO2 electroreduction: A review. *Renewable and Sustainable Energy Reviews* **2024**, *206*, 114869.
(16) Möhle, S.; Zirbes, M.; Rodrigo, E.; Gieshoff, T.; Wiebe, A.; Waldvogel, S. R. Modern Electrochemical Aspects for the Synthesis of Value-Added Organic Products. *Angew. Chem., Int. Ed.* **2018**, *57* (21), 6018−6041.
(17) Jin, S.; Hao, Z.; Zhang, K.; Yan, Z.; Chen, J. Advances and Challenges for the Electrochemical Reduction of CO2 to CO: From Fundamentals to Industrialization. *Angew. Chem., Int. Ed.* **2021**, *60* (38), 20627−20648.
(18) Han, J.; Bai, X.; Xu, X.; Bai, X.; Husile, A.; Zhang, S.; Qi, L.; Guan, J. Advances and challenges in the electrochemical reduction of carbon dioxide. *Chemical Science* **2024**, *15* (21), 7870−7907.
(19) Salzberg, H. W. Cathodic Lead Disintegration and Hydride Formation. *J. Electrochem. Soc.* **1953**, *100* (4), 146.
(20) Gastwirt, L. W.; Salzberg, H. W. Disintegration of Lead Cathodes, II. *J. Electrochem. Soc.* **1957**, *104* (12), 701.
(21) Wirtanen, T.; Prenzel, T.; Tessonnier, J.-P.; Waldvogel, S. R. Cathodic Corrosion of Metal Electrodes—How to Prevent It in Electroorganic Synthesis. *Chem. Rev.* **2021**, *121* (17), 10241−10270.
(22) Salzberg, H. W.; Mies, F. Cathodic Disintegration of Tin. *J. Electrochem. Soc.* **1958**, *105* (2), 64.
(23) Pavesi, D.; van de Poll, R. C. J.; Krasovic, J. L.; Figueiredo, M.; Gruter, G.-J. M.; Koper, M. T. M.; Schouten, K. J. P. Cathodic Disintegration as an Easily Scalable Method for the Production of Sn- and Pb-Based Catalysts for CO2 Reduction. *ACS Sustainable Chem. Eng.* **2020**, *8* (41), 15603−15610.
(24) Salzberg, H. W.; Andreatch, A. J. Evolution of Stibine at Antimony Cathodes. *J. Electrochem. Soc.* **1954**, *101* (10), 528.
(25) Pitman, A. L.; Pourbaix, M.; de Zoubov, N. Potential-pH Diagram of the Antimony-Water System: Its Applications to Properties of the Metal, Its Compounds, Its Corrosion, and Antimony Electrodes. *J. Electrochem. Soc.* **1957**, *104* (10), 594.
(26) Dukovic, J.; Tobias, C. W. The Influence of Attached Bubbles on Potential Drop and Current Distribution at Gas-Evolving Electrodes. *J. Electrochem. Soc.* **1987**, *134* (2), 331.
(27) Ross, B.; Haussener, S.; Brinkert, K. Impact of Gas Bubble Evolution Dynamics on Electrochemical Reaction Overpotentials in Water Electrolyser Systems. *J. Phys. Chem. C* **2025**, *129* (9), 4383−4397.
(28) Lake, J. R.; Soto, Á. M.; Varanasi, K. K. Impact of Bubbles on Electrochemically Active Surface Area of Microtextured Gas-Evolving Electrodes. *Langmuir* **2022**, *38* (10), 3276−3283.
(29) Haber, F. The phenomenon of the formation of metallic dust from cathodes. *Trans. Am. Electrochem. Soc.* **1902**, *2*, 189−196.
(30) Campari, A.; Ustolin, F.; Alvaro, A.; Paltrinieri, N. A review on hydrogen embrittlement and risk-based inspection of hydrogen technologies. *International Journal of Hydrogen Energy* **2023**, *48* (90), 35316−35346.
(31) Roberts, E. W. Space tribology: its role in spacecraft mechanisms. *J. Phys. D: Appl. Phys.* **2012**, *45* (50), 503001.
(32) Gale, W. F.; Totemeier, T. C. *Smithells Metals Reference Book*; Butterworth-Heinemann, 2003.
(33) Papanikolaou, N. C.; Hatzidaki, E. G.; Belivanis, S.; Tzanakakis, G. N.; Tsatsakis, A. M. Lead toxicity update. A brief review. *Med. Sci. Monit.* **2005**, *11* (10), RA329−RA336.
(34) Hersbach, T. J. P.; McCrum, I. T.; Anastasiadou, D.; Wever, R.; Calle-Vallejo, F.; Koper, M. T. M. Alkali Metal Cation Effects in Structuring Pt, Rh, and Au Surfaces through Cathodic Corrosion. *ACS Appl. Mater. Interfaces* **2018**, *10* (45), 39363−39379.
(35) Liu, S.; Li, Y.; Wang, D.; Xi, S.; Xu, H.; Wang, Y.; Li, X.; Zang, W.; Liu, W.; Su, M.; et al. Alkali cation-induced cathodic corrosion in Cu electrocatalysts. *Nat. Commun.* **2024**, *15* (1), 5080.
(36) Bender, J. T.; Petersen, A. S.; Østergaard, F. C.; Wood, M. A.; Heffernan, S. M. J.; Milliron, D. J.; Rossmeisl, J.; Resasco, J. Understanding Cation Effects on the Hydrogen Evolution Reaction. *ACS Energy Lett.* **2023**, *8* (1), 657−665.
(37) Baizer, M. M. Electrolytic Reductive Coupling: I. Acrylonitrile. *J. Electrochem. Soc.* **1964**, *111* (2), 215.
(38) Mast, F.; Hielscher, M. M.; Wirtanen, T.; Erichsen, M.; Gauss, J.; Diezemann, G.; Waldvogel, S. R. Choice of the Right Supporting Electrolyte in Electrochemical Reductions: A Principal Component Analysis. *J. Am. Chem. Soc.* **2024**, *146* (22), 15119−15129.
(39) Mousavi, M. P. S.; Kashefolgheta, S.; Stein, A.; Bühlmann, P. Electrochemical Stability of Quaternary Ammonium Cations: An Experimental and Computational Study. *J. Electrochem. Soc.* **2016**, *163* (2), H74.
(40) Mast, F.; Hielscher, M. M.; Plut, E.; Gauss, J.; Diezemann, G.; Waldvogel, S. R. Quaternary Ammonium Salts as Supporting

Electrolytes in Cathodic Reductions: An Analysis of Their Electrochemical Stability. *J. Phys. Chem. B* **2025**, *129* (25), 6241−6252.
(41) Mathison, R.; Atwi, R.; McConnell, H. B.; Ochoa, E.; Rani, E.; Akashige, T.; Röhr, J. A.; Taylor, A. D.; Avalos, C. E.; Aydil, E. S.; et al. Molecular Processes That Control Organic Electrosynthesis in Near-Electrode Microenvironments. *J. Am. Chem. Soc.* **2025**, *147* (5), 4296−4307.
(42) Dubouis, N.; Grimaud, A. The hydrogen evolution reaction: from material to interfacial descriptors. *Chemical Science* **2019**, *10* (40), 9165−9181.
(43) Edinger, C.; Kulisch, J.; Waldvogel, S. R. Stereoselective cathodic synthesis of 8-substituted (1R,3R,4S)-menthylamines. *Beilstein Journal of Organic Chemistry* **2015**, *11*, 294−301.
(44) Edinger, C.; Waldvogel, S. R. Electrochemical Deoxygenation of Aromatic Amides and Sulfoxides. *European Journal of Organic Chemistry* **2014**, *2014* (24), 5144−5148.
(45) Kulisch, J.; Nieger, M.; Stecker, F.; Fischer, A.; Waldvogel, S. R. Efficient and Stereodivergent Electrochemical Synthesis of Optically Pure Menthylamines. *Angew. Chem., Int. Ed.* **2011**, *50* (24), 5564−5567.
(46) Schwetlick, K. *Organikum: Organisch-chemisches Grundpraktikum*, 24 Auflage; WILEY_VCH, 2015.
(47) Dell'Anna, M. N.; Gupta, G.; Prabhu, P. T.; Chu, T.-H.; Roling, L. T.; Tessonnier, J.-P. Local reactivity descriptors to decipher the electrochemical hydrogenation of unsaturated carboxylic acids. *Green Chem.* **2023**, *25* (24), 10387−10397.
(48) Escanio, C. A.; S dos Santos, S.; M Natale, J.; A de L Almeida, D.; Trava-Airoldi, V. J.; Corat, E. J. Polyaniline-Lead Composites as Inhibitors for the Hydrogen Evolution Reaction, Relevant for Lead-Acid Batteries. *J. Phys. Chem. C* **2024**, *128* (13), 5490−5504.
(49) Jiang, Z.; Wang, T.; Song, L.; Guo, H.; Xia, W.; Gong, H.; Gao, B.; Feng, L.; Liu, X.; He, J. High over-potential nitrogen-doped activated carbon towards hydrogen evolution inhibition in sulfuric acid solution. *Journal of Materials Science: Materials in Electronics* **2018**, *29* (16), 14170−14179.
(50) Li, Y.; Wang, F.; Liu, G. Grain Size Effect on the Electrochemical Corrosion Behavior of Surface Nanocrystallized Low-Carbon Steel. *Corrosion* **2004**, *60* (10), 891−896.
(51) Moreno-García, P.; Gálvez-Vázquez, M. d. J.; Prenzel, T.; Winter, J.; Gálvez-Vázquez, L.; Broekmann, P.; Waldvogel, S. R. Self-Standing Metal Foam Catalysts for Cathodic Electro-Organic Synthesis. *Advanced Materials* **2024**, *36* (9), 2307461.
(52) Delahay, P.; Pourbaix, M.; Rysselberghe, P. V. Potential-pH Diagram of Lead and its Applications to the Study of Lead Corrosion and to the Lead Storage Battery. *J. Electrochem. Soc.* **1951**, *98* (2), 57.
(53) Bender, J.; Uvodich, A.; Valles, A.; Milliron, D.; Resasco, J. Surface Charge Universally Predicts the Presence of Cation Effects in Electrocatalysis. *ChemRxiv* **2025**, 2025-t7g2f.
(54) Yang, Z.; Zhan, F.; Pan, Y.; Lyu, Z.; Han, C.; Hu, Y.; Ding, P.; Gao, T.; Zhou, X.; Jiang, Y. Structure of a novel Benzyl Quinolinium Chloride derivative and its effective corrosion inhibition in 15wt.% hydrochloric acid. *Corrosion Science* **2015**, *99*, 281−294.
(55) Koushik, A. K. S.; Finley, D.; Intan, N. N.; Showman, L. J.; Podolak, K.; Crandall, Z.; Windus, T. L.; Pfaendtner, J.; Waldvogel, S. R.; Kraus, G. A.; et al. A Platform Approach for Designing Sustainable Indole Thiosemicarbazone Corrosion Inhibitors with Enhanced Adsorption Properties. *Langmuir* **2025**, *41* (12), 8407−8423.
(56) Levich, V. G.; Tobias, C. W. Physicochemical Hydrodynamics. *J. Electrochem. Soc.* **1963**, *110* (11), 251C.
(57) Li, J.; Li, X.; Gunathunge, C. M.; Waegele, M. M. Hydrogen bonding steers the product selectivity of electrocatalytic CO reduction. *Proc. Natl. Acad. Sci. U. S. A.* **2019**, *116* (19), 9220−9229.
(58) Dunwell, M.; Luc, W.; Yan, Y.; Jiao, F.; Xu, B. Understanding Surface-Mediated Electrochemical Reactions: CO2 Reduction and Beyond. *ACS Catal.* **2018**, *8* (9), 8121−8129.
(59) McCrum, I. T.; Hickner, M. A.; Janik, M. J. Quaternary Ammonium Cation Specific Adsorption on Platinum Electrodes: A Combined Experimental and Density Functional Theory Study. *J. Electrochem. Soc.* **2018**, *165* (2), F114.




https://doi.org/10.1021/acselectrochem.5c00398
*ACS Electrochem.* 2026, 2, 175−187